# Electronic Supplementary Material

# Robust scalable reversible strong adhesion by gecko-inspired composite design

**Xiaosong LI, Pengpeng BAI, Xinxin LI, Lvzhou LI, Yuanzhe LI, Hongyu LU, Liran MA*, Yonggang MENG, Yu TIAN***

*State Key Laboratory of Tribology, Department of Mechanical Engineering, Tsinghua University, Beijing 100084, China*

Supporting information to https://doi.org/10.1007/s40544-021-0522-4

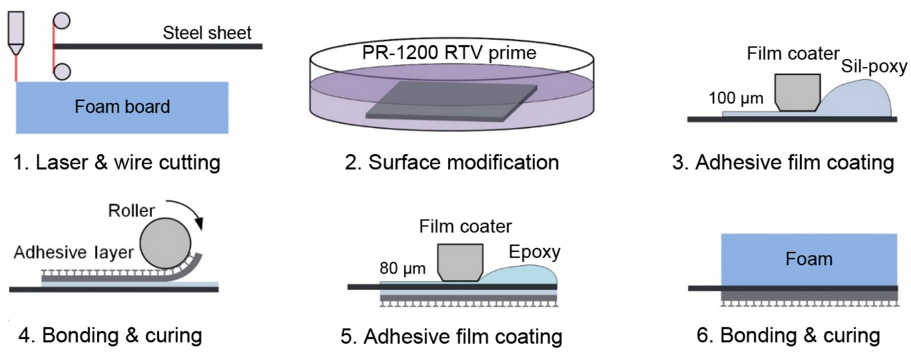


**Fig. S1** Schematic illustrations of the experimental procedure for fabricating PSCU.

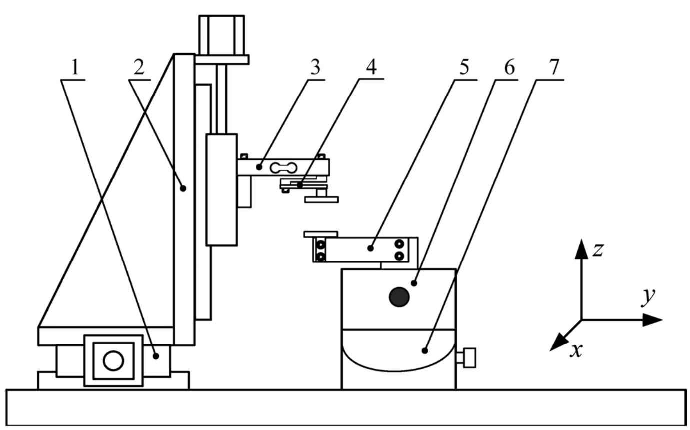


**Fig. S2** Schematic illustration of the experiment setup. 1: $x$-axis motorized translation stage; 2: $z$-axis motorized translation stage; 3: Normal cantilever force sensor; 4: Protective buffer; 5: Tangential cantilever force sensor; 6: $y$-axis angular adjustment stage; 7: $x$-axis angular adjustment stage.

### Detachment behaviors in adhesion and peeling tests

To reveal the actual detachment behaviors in adhesion and peeling tests, corresponding contact states of

* Corresponding authors: Yu TIAN, E-mail: tianyu@mail.tsinghua.edu.cn; Liran MA, E-mail: maliran@mail.tsinghua.edu.cn

individual pillars in the back-pulling process (Vedio S1) and the edge-peeling process (Vedio S2) were recorded. Both processes could be divided into four phases (Figs. S3 and S4). In the initial phase, the adhesive unit contacts the substrate with a proper preload (Figs. S3(a) and S4(a)). During the back-pulling process, all the pillars are stretched simultaneously, i.e., load sharing. The microscopic crack initiates from the center of each pillar and propagates with the adhesion force increasing [S1–S3], as marked in one red circle for reference (Fig. S3(c)). When most pillars reach the maximum adhesion strength simultaneously, the adhesive unit is suddenly separated from the substrate, accompanied by strong adhesion.

In the edge-peeling process, the pillars adjacent to the peel front are the first portion to be stretched. In contrast, the pillars away from the peel front are compressed due to steel sheet bending. The pillar shaft is compressed to be darker in the center while the outer thin plate is lighter (Fig. S4(b)). With the peeling distance increasing, the initiated macroscopic crack (peel front) at the edge gradually propagates to the observing area (Fig. S4(c)). The stretched area is also called the peel zone (of the whole adhesive unit), which moves along with the peel front when the tensile stress of the stretched pillars exceeds the adhesion strength [S4, S5]. After the pre-peeling, much fewer numbers of attached pillars promised the easy detachment afterward.

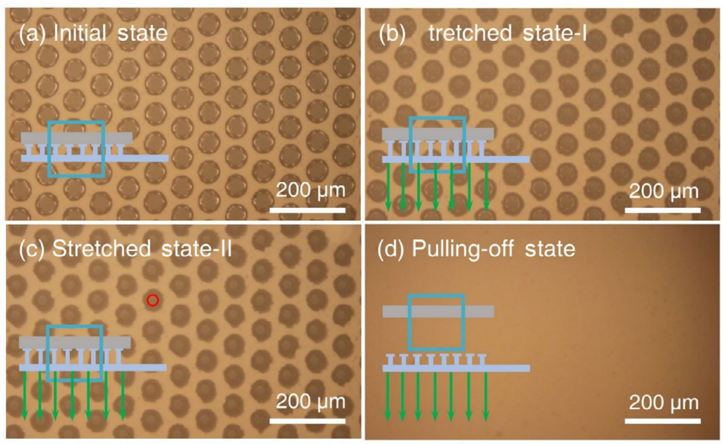


**Fig. S3** Microscopic observation of the contact state evolution between the mushroom-shaped adhesive surface and glass substrate during the back-pulling process. The pillars in the observing area went through (a) initial state, (b) slightly stretched state, (c) severely stretched state, and (d) pulling-off state, successively. The inserted schematics show the corresponding contact states. The blue box and the green arrow indicate the observing area and adhesion force, respectively.

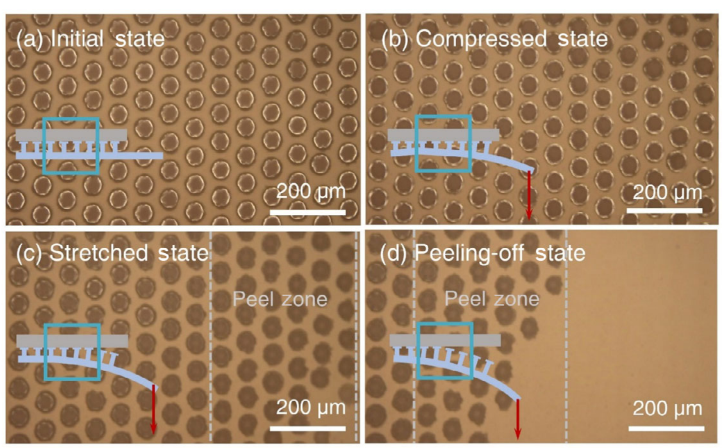


**Fig. S4** Microscopic observation of the contact states between the mushroom-shaped adhesive surface and glass substrate during the edge-peeling process. The pillars in the observing area went through (a) initial state, (b) compressed state, (c) stretched state, and (d) peeling-off state, successively. The inserted schematics show the corresponding contact states. The blue box and the red arrow indicate the observing area and peeling force, respectively.

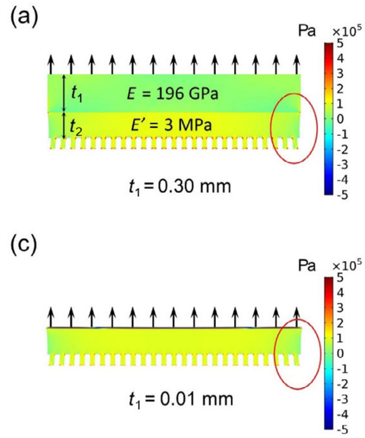


**Fig. S5** Normal stress and deformation distribution of the steel sheet and the adhesive layer with an applied normal stress of 100 kPa. The red circle marked the lateral shrinkage of the 0.2 mm thick adhesive layer with different thicknesses of steel sheet, which indicated that the high-elastic-modulus steel sheet restrains the shrinkage of adhesive layer in the loading area.

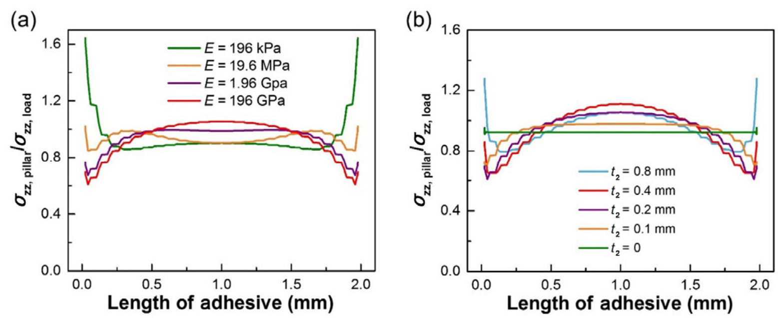


**Fig. S6** 2D plane-strain simulation results of tensile stresses distribution in pillars along the adhesive layer length direction. Results for (a) different Young's modulus of steel sheet, $E$, and (b) different thicknesses of adhesive layer $t_2$. The data were taken from the middle nodes of the pillars and normalized by dividing the local stress by the applied homogeneous normal stress.

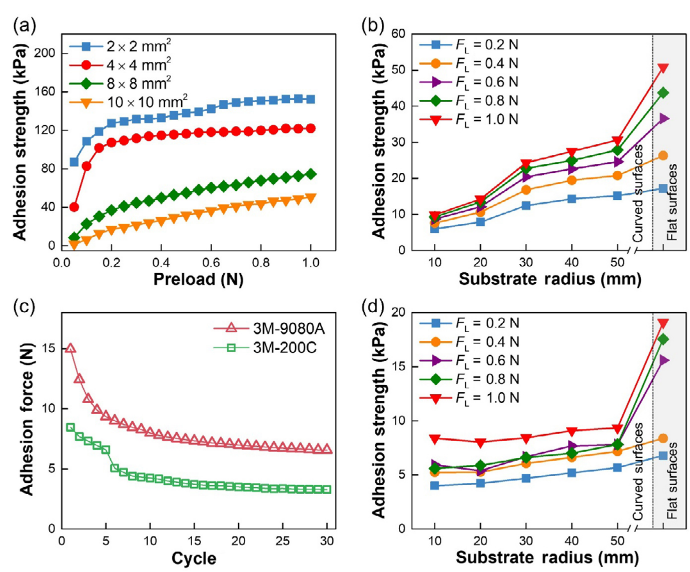


**Fig. S7** Adhesion force test results. (a) Adhesion force test between mushroom-shaped adhesive surface with different sizes and flat glass substrate. (b) Adhesion force test between mushroom-shaped adhesive surface and spherical glass substrate with different curvature radii under various preloads. (c) The repeatability tests of commercial PSAs including 3M-9080A and 3M-200C. (d) The adhesion strength tests between commercial 3M-200C adhesive tape and spherical glass substrate with different curvature radii under various preloads.

**Theoretical analysis of peeling force and related design considerations**

To give a detailed relationship between the geometry and material properties of the backing steel sheet and the peeling force, a theoretical model was established based on the bending beam theory and the principle of minimum potential energy [S6], as shown in Fig. S8. To simplify the model, all the pillars are assumed to be stretched perpendicularly to the substrate, and they are separated from the substrate when the tensile stress exceeds the maximum adhesion strength. Besides, the tensile stress in the peel zone of the adhesive layer is assumed to be in a linear distribution along the length direction of the steel sheet, as the area of all the stretched pillars is small in contrast to the steel sheet. In addition, the bending stiffness of the adhesive layer is too low to be neglected, in contrast to the steel sheet.

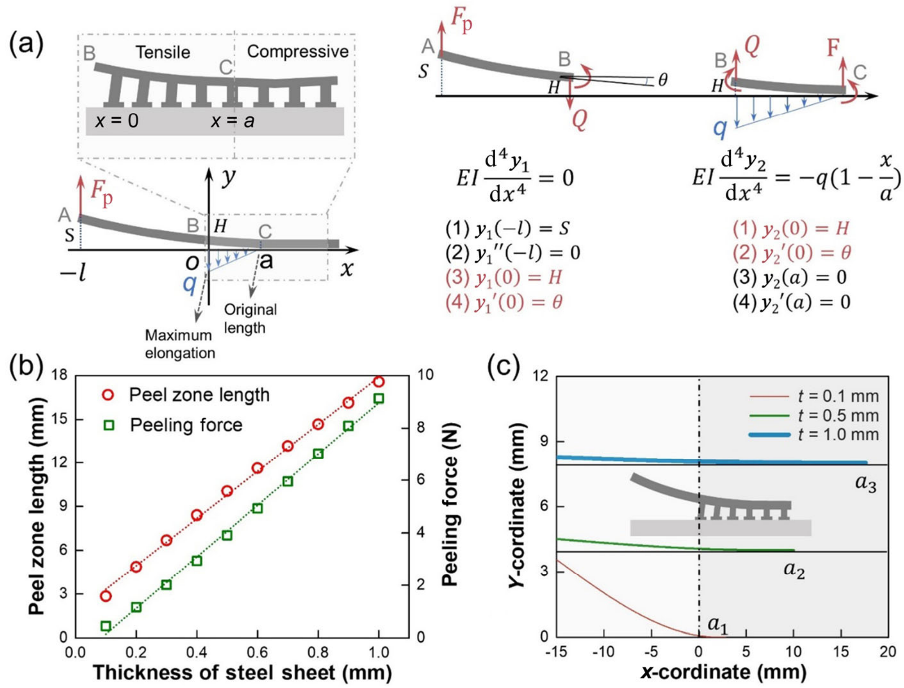


**Fig. S8** Analytical model and calculated results of the mushroom-shaped adhesive layer bonded with a steel sheet. (a) Schematic of a simplified model based on the bending beam theory, and related governing equations and boundary conditions. (b) Peel zone length and corresponding peeling force depending on the thickness of steel sheet. (c) The displacement field curves of the bending steel sheet at the end of the crack initiation phase for different steel sheet thickness *t*.

Generally, the peeling process could be divided into crack initiation and crack propagation. The peeling force increases almost linearly to the peak value until a macroscopic crack initiated at the edge of the adhesive interface. Then the crack propagates gradually to the other end, accompanied by the decrease of interfacial stiffness and peeling force, as shown in Fig. S9. The crack initiation phase is regarded as a quasi-static process. The peeling force $F_P$ and the peel zone length $a$ are determined when the peeling distance $S$ is given. To solve the peeling force, we need to obtain the displacement field of the whole steel sheet, especially when the first stretched pillar at the crack front is going to separate from the substrate. The adhesive unit is divided into two parts to solve the whole displacement field, as shown in Fig. S8(a). The demarcation is defined as point B, where the pillars are stretched to the maximum elongation. The endpoint of the right part is defined as point C, where the pillars remain the original length. The differential equation of the left part AB is

$$\frac{d^4y_1}{dx^4} = 0 \tag{1}$$

whose solution fulfills the boundary conditions $y_1(-l)=S$, $y_1''(-l)=0$, $y_1(0)=H$, and $y_1'(0)=\theta$, where $S$ is the peeling distance, $H$ is the maximum elongation of the pillar, and $\theta$ is the angle at point B induced by the moment. For the right part BC, the differential equation is

$$E_{\text{steel}} I \frac{\mathrm{d}^4 y_2}{\mathrm{d}x^4} = -q(1-x/a) \tag{2}$$

whose solution fulfills the boundary conditions $y_2(0)=H$, $y_2'(0)=\theta$, $y_2(a)=0$, and $y_2'(a)=0$, where $a$ is the peel zone length and $q$ is the maximum adhesive load intensity. Considering the continuity conditions of moment and shearing force at the original point O, which can be interpreted as $y_1''(0)=y_2''(0)$ and $y_1'''(0)=y_2'''(0)$, the intermediate variables $H$ and $\theta$ could be replaced by $S$ and $a$, respectively. The strain energy ($U_\text{e}$) of the system can be derived as the sum of the bend strain energy of the steel sheet ($U_{\text{s,b}}$) and the stretch strain energy of the pillars ($U_{\text{p,s}}$), and that of the soft backing layer ($U_{\text{b,s}}$) yields

$$U_\text{e} = U_{\text{s,b}} + U_{\text{p,s}} + U_{\text{b,s}} \tag{3}$$

Since the bending stiffness of the adhesive layer is neglected, the total bend energy should be expressed as

$$U_{\text{s,b}} = \frac{1}{2}\int_{-1}^{0} E_{\text{steel}} I \left(\frac{\mathrm{d}^2 y_1}{\mathrm{d}x^2}\right)^2 \mathrm{d}x + \frac{1}{2}\int_{0}^{a} E_{\text{steel}} I \left(\frac{\mathrm{d}^2 y_2}{\mathrm{d}x^2}\right)^2 \mathrm{d}x \tag{4}$$

To simplify the calculation, all the pillars are hypothetically considered as springs with an equivalent spring coefficient $k$, which can be expressed as

$$k = E_{\text{PVS}} A/h \tag{5}$$

where $A = \pi d^2/4$ is the cross-sectional area of the pillar, $d$ is the pillar diameter. By considering the hexagonal distribution of the pillars, the equivalent stretch energy of the whole area could be written as

$$U_{\text{p,s}} = \frac{\sqrt{3}}{3}\frac{k}{(\Delta d)^2}\int_0^a y_2^2 \mathrm{d}x \tag{6}$$

where $\Delta d$ is the distance between the centers of pillars, $d$ is the pillar diameter. By considering a unit cell of soft backing in series with a pillar, we can estimate the stretch strain energy of the soft backing layer as $U_{\text{b,s}} = U_{\text{p,s}}$ to simplify its calculation.

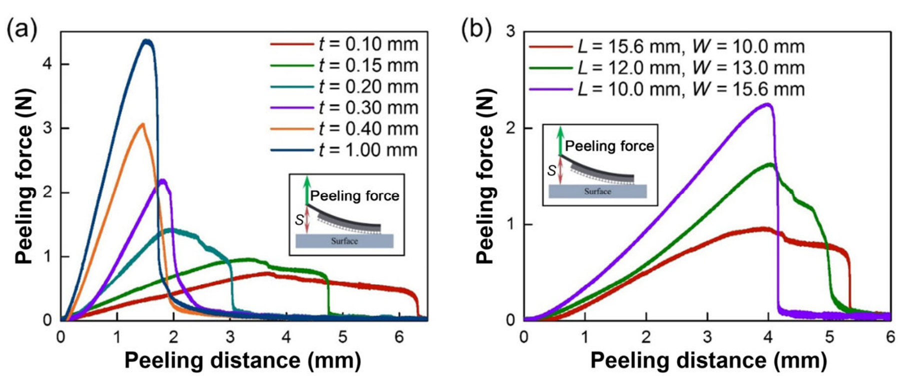


**Fig. S9** Peeling force of the adhesive surface versus peeling distance of steel sheet by the releasing tendon. The length and width of the steel sheet in (a) are 15.6 and 10 mm, respectively. The thickness of the steel sheet in (b) is 0.15 mm. All the peeling speed of the releasing tendon is 0.1 mm/s. The schematic insets represent the corresponding contact states from the side view.

Since the peeling distance $S$ is selected as the control parameter, the corresponding peel zone length $a$ can be obtained when the principle of minimum potential energy is satisfied, as given by

$$\frac{\partial U_{\mathrm{e}}}{\partial a}=0 \tag{7}$$

Consequently, the displacement field of the whole steel sheet can be obtained when $S$ is given, and the corresponding peeling force can be calculated as

$$F_{\mathrm{p}}=E_{\mathrm{steel}}I\frac{\mathrm{d}^3y_1(0)}{\mathrm{d}x^3} \tag{8}$$

Note that the calculated energy and peeling force are for adhesive units with a unit width. And the final value was transformed to match the actual width $b$. When the maximum adhesive load intensity $q$ reaches the maximum adhesion strength criterion $P_{\mathrm{ad}}$, i.e., the first pillar is going to separate from the substrate, the calculated $F_{\mathrm{P}}$ satisfies the corresponding maximum peeling force. The values of all the parameters used in the theoretical model are given in Table S1.

**Table S1** Parameters of the analytical model for the mushroom-shaped adhesive and steel sheet.

| | | |
|---|---|---|
| Pillar diameter | $d$ | 40 μm |
| Pillar height | $h$ | 80 μm |
| Distance between pillars | $\Delta d$ | 60 μm |
| Distance from the terminal of steel sheet to the first stretching pillar | $l$ | 15 mm |
| Width of the steel sheet | $b$ | 12 mm |
| Young's modulus of the adhesive surface | $E_{\mathrm{pvs}}$ | 3 MPa |
| Young's modulus of the steel sheet | $E_{\mathrm{steel}}$ | 196 GPa |
| Maximum adhesion strength criterion | $P_{\mathrm{ad}}$ | ~300 kPa |

In the crack propagation phase, the Griffith criterion is satisfied to be in stable equilibrium as

$$\frac{\partial}{\partial a}(-W_{\mathrm{e}}+U_{\mathrm{e}}+U_{\mathrm{s}})=0 \tag{9}$$

where $W_{\mathrm{e}}=\int_0^s F_{\mathrm{p}}\mathrm{d}S$ equals to the work done by the peeling force, $U_{\mathrm{e}}=U_{\mathrm{s,b}}+U_{\mathrm{p,s}}$ equals to the elastic energy stored in the bent steel sheet and the stretched pillars, and $U_{\mathrm{s}}=\gamma wa$ equals to the increased surface energy that resulted from crack propagation. To advance the crack, the Griffith equation could be interpreted as

$$G_{\mathrm{L}}=W_{\mathrm{ad}}\ \left(\frac{\mathrm{d}G_L}{\mathrm{d}a}<0\right) \tag{10}$$

where $G_{\mathrm{L}}=\frac{\mathrm{d}W_{\mathrm{e}}}{\mathrm{d}a}-\frac{\mathrm{d}U_{\mathrm{e}}}{\mathrm{d}a}$ represents local energy releasing rate, which is the difference between input energy rate and stored strain energy rate [S7]. The observed bending radius close to the crack tip for thick steel sheet was gradually increasing with crack propagation. Therefore, the bending strain energy was released to propagate the crack, i.e., $\frac{\mathrm{d}U_{\mathrm{e}}}{\mathrm{d}a}<0$. More specifically, under the same peeling speed, the crack propagation speed increases with the bending stiffness (Fig. S9). Because a steel sheet with higher stiffness stores more energy under the same deformation, thereby leading to higher energy releasing rate for deformation recovery.

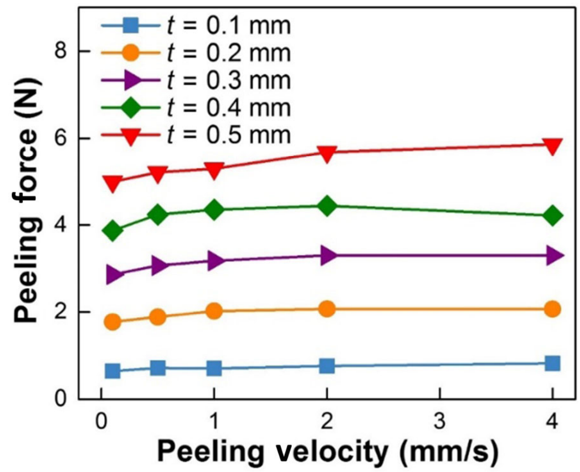


**Fig. S10** Effects of peeling velocity on the peeling force of the adhesive unit.

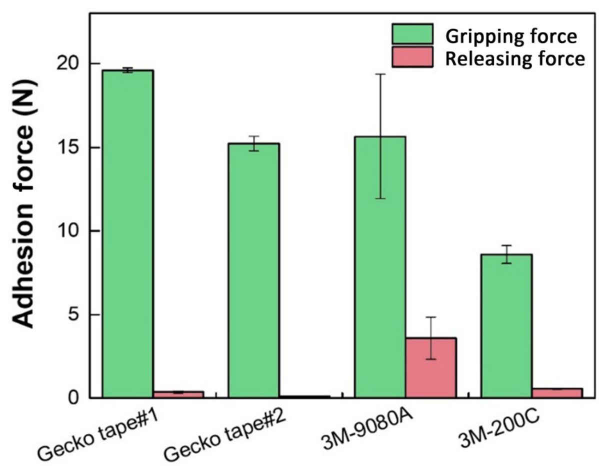


**Fig. S11** Gripping forces and releasing forces of PSCUs with different adhesive layers. Gecko tape#1 is the mushroom-shaped adhesive surface described in the experimental section. Gecko tape#2 is our self-made mushroom-shaped adhesive surface with PDMS by conventional photolithography [S3], which has different pillar sizes from Gecko tape#1. 3M-9080A and 3M-200C are commercial PSAs purchased from 3M Co., Ltd. The adhesive area of all these samples remains constant at 1.5 $cm^2$ and the preload is 5 N.

**Vedio S1** Detachment behaviors of micropillars in the process of pulling from the back of the steel sheet.

**Vedio S2** Detachment behaviors of micropillars in the process of peeling from the edge of the steel sheet.

**Vedio S3** Demonstration of the four-legged gripper utilizing switchable strong adhesion to pick and place both a DC power supply with flat surfaces and a football with curved surfaces. The DC power supply has a length of 30 cm, a width of 13 cm, and a height of 16 cm. The football size is 22 cm in diameter.

**Vedio S4** Demonstration of the four-legged gripper integrated on a robot arm utilizing switchable strong adhesion to pick up, transfer, and release a 3.2 kg flat mass with a speed of ~60 mm/s.

**Vedio S5** Demonstration of utilizing a 103 g gripper based on the sandwiched composite unit to lift up and drop down a 6.3 kg flat mass without applying any external load for engagement. The adhesive area of this gripper is about 8 $cm^2$.

**Vedio S6** Demonstration of the four-legged robot utilizing switchable strong adhesion to walk upside down on a glass ceiling.

**Vedio S7** Demonstration of the developed ceiling-climbing gripper enabling a 70 kg adult to hang on a glass ceiling stably while to release easily with a low detachment force. Note that it was so difficult for an adult to climb on an inverted ceiling with only one arm that only the reversibility of this climbing gripper was demonstrated.

## References


[S1] Gorb S, Varenberg M, Peressadko A, Tuma J. Biomimetic mushroom-shaped fibrillar adhesive microstructure. *J Royal Soc Interface* **4**(13): 271–275 (2007)

[S2] Carbone G, Pierro E, Gorb S N. Origin of the superior adhesive performance of mushroom-shaped microstructured surfaces. *Soft Matter* **7**(12): 5545 (2011)

[S3] Hu H, Tian H M, Shao J Y, Wang Y, Li X M, Tian Y, Ding Y C, Lu B H. Friction contribution to bioinspired mushroom-shaped dry adhesives. *Adv Mater Interfaces* **4**(9): 1700016 (2017)

[S4] Pesika N S, Tian Y, Zhao B X, Rosenberg K, Zeng H B, McGuiggan P, Autumn K, Israelachvili J N. Peel-zone model of tape peeling based on the gecko adhesive system. *J Adhesion* **83**(4): 383–401 (2007)

[S5] Zhou M, Pesika N, Zeng H, Wan J, Zhang X, Meng Y, Wen S, Tian Y. Design of gecko-inspired fibrillar surfaces with strong attachment and easy-removal properties: a numerical analysis of peel-zone. *J R Soc Interface* **9**(75): 2424–2436 (2012)

[S6] Popov V L. *Contact Mechanics and Friction*. Heidelberg (Germany): Springer-Verlag Berlin Heidelberg, 2010.

[S7] Glassmaker NJ, Jagota A, Hui CY, Noderer WL, Chaudhury MK. Biologically inspired crack trapping for enhanced adhesion. *PNAS* **104**(26): 10786–10791 (2007)